Autonomous Planning and Intraoperative Augmented Reality Navigation for Neurosurgery

Christian Kunz, Michal Hlaváč, Max Schneider, Andrej Pala, Pit Henrich, Birgit Jickeli, Heinz Wörn, Björn Hein, Rainer Wirtz, and Franziska Mathis-Ullrich

***Abstract*—Neurosurgical interventions in the brain are challenging due to delicate anatomical structures. During surgery, precise navigation of surgical instruments supports surgeons and allows prevention of adverse events. Here, an augmented reality-based navigation aid with automated segmentation of risk structures and path planning is presented. Superimposed patient models are visualized during neurosurgical interventions on the example of the ventricular puncture. The proposed system is experimentally validated in a realistic operating room scenario with expert neurosurgeons to determine its quality of support as well as its potential for clinical translation. The automated segmentation reaches a F1-Score of 95-99%. Paths are planned correctly in 93.4%. The entire process enables navigation aid in under five minutes. Validation shows that the system allows for a puncture success rate of 81.7% with mean accuracy of 4.8 ± 2.5 mm. A control group who performed the standard-of-care procedure reached a rate of 71.7% with 6.5 ± 2.4 mm accuracy. Acceptability analysis shows that 85.7% of the participating surgeons approve of the system's convenience and 92.9% expect accuracy improvement. The presented navigation aid for ventricular puncture enables automated surgical planning and may improve accuracy and success rates of neurosurgical interventions.**

***Index Terms*—Augmented reality (AR), ventricular drain placement, computer assisted surgery, surgical planning, surgical navigation.**

Manuscript received March 10, 2021; revised April 8, 2021; accepted May 31, 2021. Date of publication June 22, 2021; date of current version August 26, 2021. This article was recommended for publication by Associate Editor M. Hashizume and Editor P. Dario upon evaluation of the reviewers' comments. This work was supported by the German Federal Ministry of Education and Research under Grant 01IS17005. *(Corresponding author: Franziska Mathis-Ullrich.)*

This work did not involve human subjects or animals in its research.

Christian Kunz, Pit Henrich, Birgit Jickeli, Heinz Wörn, and Franziska Mathis-Ullrich are with the Health Robotics and Automation Lab, Institute for Anthropomatics and Robotics, Karlsruhe Institute of Technology, 76131 Karlsruhe, Germany (e-mail: franziska.ullrich@kit.edu).

Michal Hlaváč, Max Schneider, Andrej Pala, and Rainer Wirtz are with the Department of Neurosurgery, University of Ulm, 89081 Günzburg, Germany.

Björn Hein is with the Intelligent Industrial Robotics Group, Institute for Anthropomatics and Robotics, Karlsruhe Institute of Technology, 76131 Karlsruhe, Germany, and also with the Research Group Robotics and Autonomous Systems, University of Applied Sciences, 76133 Karlsruhe, Germany.

This article has supplementary downloadable material available at https://doi.org/10.1109/TMRB.2021.3091184, provided by the authors.

Digital Object Identifier 10.1109/TMRB.2021.3091184

I. Introduction

SINCE its beginnings, neurosurgery has been on the forefront of technical innovation in medicine. This surgical discipline comprises all procedures performed on the human brain and spine, including the resection of tumors, vascular lesions, evacuation of hematoma following traumatic injury or intracranial hemorrhage, and placement of catheters into the ventricles of the brain. Due to the intricate and delicate nature of brain tissue an adherent risk of severe damage arises that may cause fatal harm to the patient. Thus, great potential arises for technologies that support neurosurgeons during their crucial work and increase the precision of surgical interventions. As the surgical target inside the brain is generally not visible during biopsies or catheter placement, procedures are often performed under the guidance of a navigation system. Since setting up such systems can be cumbersome in time-critical emergency situations, standard free-hand technique is the preferred method. As an example, during the ventricular puncture for drain placement, surgeons maintain orientation through the sense of touch by perceiving distant anatomical landmarks. Resulting catheter position is considered "optimal" in 40-77% [1]–[8]. Commercially available surgical navigation tools usually require manual planning of the catheter's entry point and insertion angle. Moreover, rigid head fixation or attachment of a marker system directly to the skull is required. Augmented reality (AR) can help visualize hidden structures, which otherwise would not be visible to the surgeon, and thus, can provide an easy-to-use navigation aid with the potential to improve the placement accuracy and minimize the risk for brain damage. The use of additional navigation aids is acceptable for neurosurgeons if the normal surgical workflow is not extended more than 10 minutes [9].

Our main goal is the demonstration of AR based surgical support during the ventricular puncture as an example for a neurosurgical intervention as seen in Fig. 1. The envisioned system uses AR glasses as the sole active component. Patient tracking is maintained with a marker system attached to the forehead of the patient non-invasively. Automated planning of the procedure with the potential to speed up the process further adds to the usability and accuracy, thus, leading to better surgical outcomes. The correct orientation for ventricular drain placement has been shown to lie perpendicular to the Kocher's point [10]. To automate trajectory planning

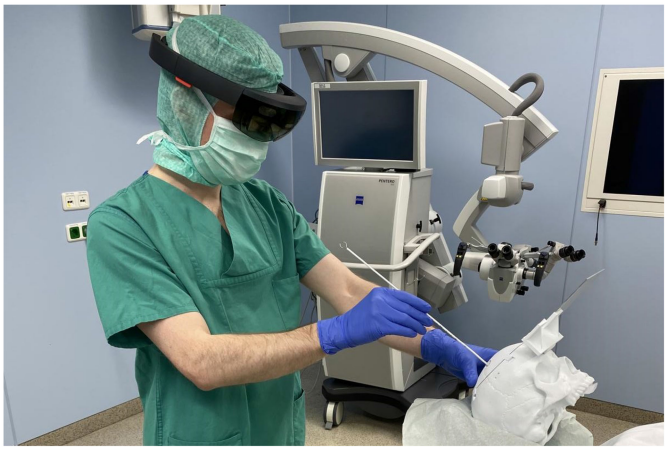

Fig. 1. Evaluation of the proposed system, showing an augmented reality supported navigation during ventriculostomy on a custom build medical phantom. The custom build phantom can be equipped with five different ventricular systems and is tracked with a Vuforia marker.

for drain placement, a template based system is presented in [11]. Automatic segmentation of computed tomography (CT) scans is still considered difficult due to the great inter-patient shape variance of organs and an unfavorable signal to noise ratio. An approach utilizing k-means clustering followed by a selection of the largest cluster to segment the ventricular system (VS) [12] has been improved by using additional morphological operators [13]. Further, template matching may extent low-level segmentation techniques [14], whereas machine learning techniques have been applied to segmentation of medical data-sets [15]. However, the discussed planning methods only cover segments of the surgical workflow, while the here proposed system covers the entire planning process from CT imaging to model generation, and trajectory planning. Every step may be supervised by a medical expert, who critically monitors the results of the automated algorithms and may intervene if required. In the past, AR systems used in a clinical environment were mainly comprised of 2D monitors, projectors, or AR in combination with microscopes [16]. Before the market launch of the Microsoft HoloLens, head mounted displays lacked the ability to be applied in surgical settings due to hardware limitations. Since then new applications have emerged. An arising challenge is characterized by tracking and registration of the patient's head during the clinical scenario.

Patients can be tracked using marker-based or markerless tracking approaches. Emerging machine learning techniques have enabled markerless tracking through landmark detection for head pose estimation [17], [18], [19]. In many cases these approaches are not applicable to the clinical environment as the patient is fully covered for sterility and patient safety. Especially in neurosurgery, features other than the surgical situs are concealed. Marker based tracking can be divided into two and three dimensional markers with a variety of 2D markers available: AprilTags [20], Aruco [21], and Vuforia (PTC Inc., MA, USA), which are capable of tracking at submillimeter range [22]. These markers are rarely applied to the medical domain due to restricted visibility and sterilizability. Frantz *et al.* [23] proposed a methodology to track a phantom utilizing Vuforia markers. The study identified marker stability with a mean drift of 1.41 mm. Infrared (IR) markers are widely used in clinical AR applications, overcoming above shortcomings. They can be sterilized and tracked from various angles. IR markers were used in combination with a hand-held video probe with augmentation of its RGB stream [24] and a projector to overlay information of underlying tumorous tissue onto the skin of a patient [25]. Various works have examined the sensor quality [26] and hologram stability of the HoloLens [27], the accuracy of placing objects in the real world, such as reference objects [28] with 1.6 mm, pedicle screw placement [29] with 4.49 mm accuracy, and a system for burr hole placement with the HoloLens with 9-16 mm accuracy. Another work uses the HoloLens for external ventricular drain placement [30]. An accuracy of 4.34 ± 1.63 mm was reached. However no patient tracking or automated planning was implemented. In addition, no coverage of the patient was used. Azimi *et al.* use Vuforia markers to track a patient during neurosurgery [31]. Prior to a CT scan fiducials are attached to the skull and later used to register the patient to the marker without automated planning of the procedure. Furthermore, model to patient registration was investigated using the HoloLens and hand gestures resulting in 98% of valid placements under 10 mm [32]. Also surface matching was used by matching patient models based on face landmark recognition combined with depth data reaching a mean accuracy of 2.2-8.6 mm [33]. Cutolo *et al.* proposed an AR-based system for neurosurgical oncology where they investigated different visualization methods [34].

In this work, a solution is proposed that comprises the complete semi-automated process of a neurosurgical procedure for placement of an external ventricular drain. The goal is to support surgeons in this operation by superimposing the patient models and navigation aids over the patient's head. As the precise tracking of the patient is of particular importance, we have developed a marker system that allows the streamlined change from the non-sterile to the sterile procedure phase. A two stage process is applied that consists of an initial coarse determination of the head position, followed by fine positioning and registration of the marker system to the patient. This process enables stable tracking of the patient during surgery. Based on the automatically generated patient models, the puncture trajectory is determined by utilizing statistical shape models to determine the trepanation point and the target area inside the VS. Navigation is offered to the surgeon in form of the patient model with integrated trajectory and landmark visualization for guidance. Our system overcomes the aforementioned limitations by providing free movement to the surgeon, a precise tracking of the patient, and support during the complete surgical workflow for external drain placement from planning to placement.

II. Material and Methods

A. System Overview

The aim of this work is to provide intuitive support to neurosurgeons without disturbing or restricting the clinical workflow. As illustrated in Fig. 2a), the proposed navigation aid consists of a marker system attached to the patient's head, several components for automated planning of the surgery

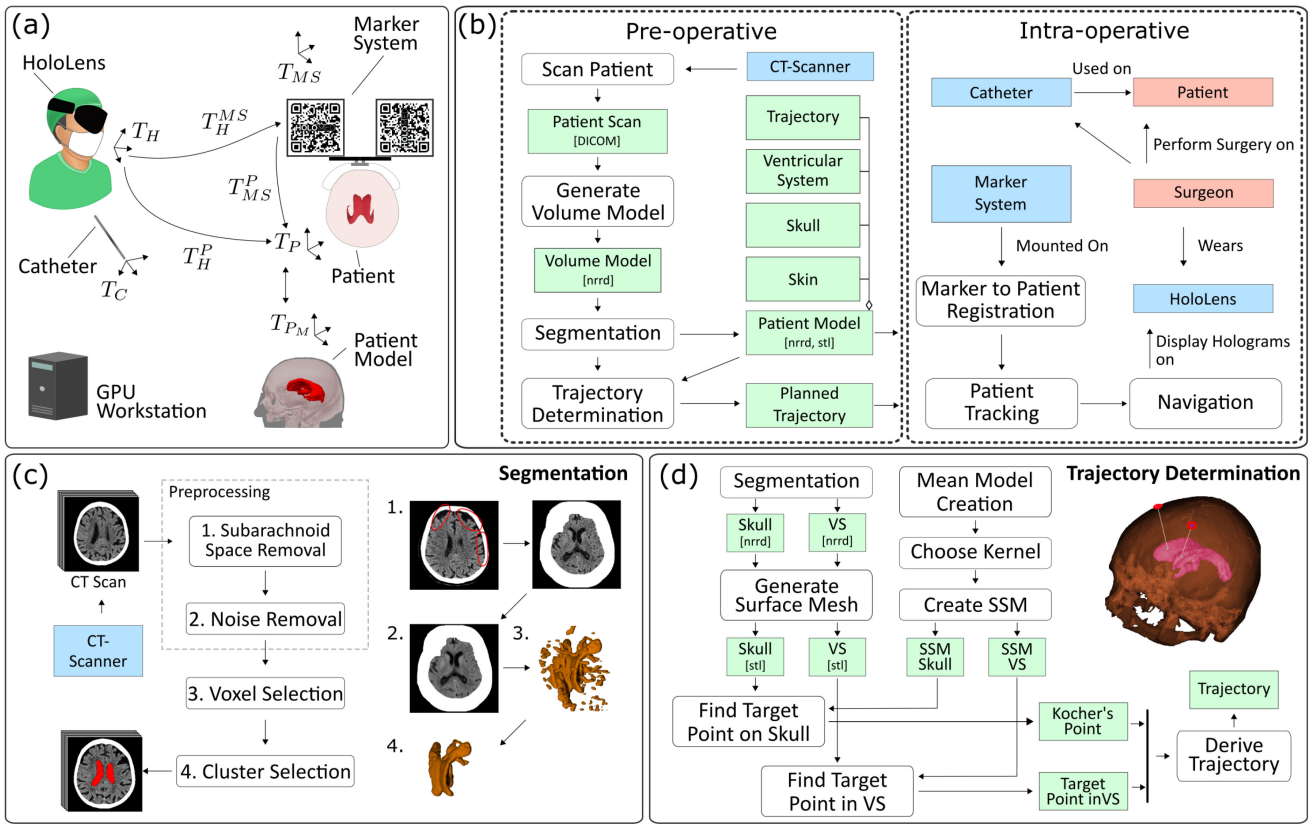

Fig. 2. (a) System overview, (b) activity diagram of the complete surgical workflow, (c) detailed process description of the automatic segmentation to derive the patient models, (d) detailed process description of the automatic trajectory determination.

such as automated generation of the patient models and trajectory determination, AR glasses (HoloLens, Microsoft Inc., USA), and a GPU workstation for processing. All planning steps for the puncture of the VS are automated and executed within a pipeline mapping the surgical workflow. Every part of the pipeline has been optimized as strict time limits must be adhered to, especially in emergency situations. An activity diagram of the whole system is depicted in Fig. 2b).

When a patient with suspected brain injury is admitted, a CT scan is performed to determine intracranial pathology, such as an enlarged VS. The proposed pipeline automatically generates the patient models from CT images including models of the skin, the skull, and the VS. Based on patient-specific data the puncture trajectory is determined by identifying the Kocher's point on the skull as well as a favorable target point within the VS. The patient models are superimposed over the patient's head during surgery using AR. Additionally, the planned trajectory is displayed as navigation aid. To display the correct hologram position in the AR device, the patient is continuously tracked during the surgical procedure. Knowledge of the relative positions allows to compensate patient movements and the parallax of the surgeon. A customized marker system is developed to track the patient that supports the change from the non-sterile to the sterile surgical phase with high assembly repeatability.

B. Automated Segmentation of Anatomical Structures

The segmentation is performed on CT scans that form a three dimensional volume of intensity values represented by Hounsfield Units (HU). The CT scan data is initially converted to the *'nrrd'* format [35] losslessly to allow easier reading and writing operations. The segmentation is later performed on these converted files. As shown in Fig. 2c), a four-step process is used to segment the VS. First, to remove existing noise and large unfavorable areas near the skull, the CT data is preprocessed. Then potential voxels of the target structures are identified and in a final step the appropriate clusters are selected. The skin and skull are also segmented using an appropriately adjusted process.

The preprocessing consists of the following steps. During physiologic ageing of the brain large bodies of fluid can accumulate between the brain tissue and the skull in the subarachnoid space. These areas and the VS are characterized with similar HU in the CT images. Thus, to simplify segmentation of the VS, the subarachnoid area is removed by growing the bone of the skull layer by layer. As the VS is located in the center of the human brain, peripheral areas can be removed safely by choosing a suitable value for the layer thickness.

To fully remove the subarachnoid space a local operator is applied iteratively until the bone has grown inward by 2.5 cm. A result is depicted in Fig. 2c) (step 1). A bilateral filter is applied to the CT data, removing high-frequency salt and pepper noise while maintaining borders, thus simplifying further image processing. After preprocessing, voxels are selected according to their corresponding HU that presumably belong to the desired structures by creating a binary mask as shown in Eq. (1). The VS is segmented utilizing a local operator. It consists mainly of cerebrospinal fluid with corresponding HU between 0 and 14. A voxel s is chosen only if a specified

fraction ($\alpha = 0.5$) of its neighborhood within a radius of 2 ($\mathcal{N}_2(s)$) voxels also lies within that range as in

$$VS(s) = \begin{cases} 1 & |\{n \in \mathcal{N}_2(s) \mid 0 \leq n_{val} \leq 14\}| \geq \alpha |\mathcal{N}_2(s)| \\ 0 & else \end{cases} \quad (1)$$

After voxel selection, the set of clusters C, which potentially represent the VS, is computed. A cluster is defined as a coherent collection of voxels. The VS is expected to be the largest homogeneous region consisting of cerebrospinal fluid (CSF) after potentially large areas of CSF in the subarachnoid space have been removed. The largest cluster M_{max} is therefore selected to represent the VS. Next, all clusters, which are at least 50% ($\beta = 0.5$) the size of M_{max}, are also included to ensure that both ventricles of a potentially disconnected VS are included. The cluster set representing the VS is finally defined as $C_{vs} = \{M \in C \mid |M| \geq \beta |M_{max}|\}$. The automated segmentation of the VS is described in more detail in [36].

Similarly, the proposed method is applied to segmentation of the skull and the skin. The approach is adapted accordingly to the respective structure. Bone has a very unique HU of 300 and higher and can thus be easily segmented from CT data utilizing a binary point operator that only takes each individual voxel into account. To segment the skin, voxels are selected in the vicinity of air. Here, the HU value range for air is assumed to be $I_a = (-\infty, -800]$, whereas that of skin is $I_s = [-750, 200]$.

In brain injury, ventricles may contain blood that cannot be segmented with a single HU range. To allow the correct selection of voxels representing fluid mixed with blood, the voxel selection criterium in Eq. (1) is extended. Multiple intervals are defined instead of a single predefined range $[min, max]$. The intervals $I_b = [0, 14] \cup [60, 80]$ result in correct voxel selection:

$$VS^{blood}(s) = \begin{cases} 1 & |\{n \in \mathcal{N}_2(s) \mid n_{val} \in I_b\}| \geq \alpha |\mathcal{N}_2| \\ 0 & else. \end{cases} \quad (2)$$

C. Automated Determination of the Puncture Trajectory

To support the surgeon during navigation of a surgical instrument, a suitable trajectory is automatically generated. The determination process is depicted in Fig. 2d.

The trajectory is described as the vector from the trepanation point (Kocher's point) to a target point inside the VS as defined in Fig. 3a. The optimal target area for the trepanation has been defined according to [7] and is illustrated in Fig. 3b. Both points are determined by utilization of statistical shape models (SSM). First, mean models of the VS and the skull are created with a gaussian kernel from 26 representative patient scans.

On these mean representations of anatomical structures, corresponding reference points for the trepanation and the target points are defined on the left/right side of the skull, as well as for the left/right lateral ventricles, respectively. The sought-after points are derived by fitting the SSMs to the patient-specific anatomy. Scalismo Lab [37] is used as a framework to create the statistical shape models and process the corresponding deformations.

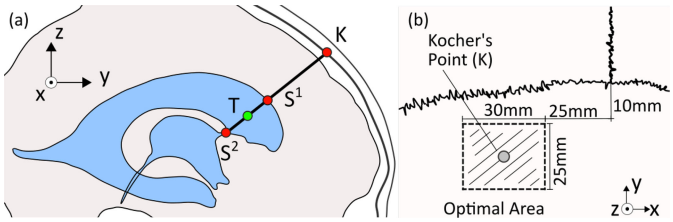

Fig. 3. (a) Determination of the target point inside the VS to retrieve the puncture trajectory, (b) Kocher's point position and acceptable puncture area.

1) Statistical Shape Model Creation: A mean shape model $\bar{x}$ is generally created from n representative meshes x_i by

$$\bar{x} = \frac{1}{n} \sum_{i=1}^{n} x_i \quad (3)$$

Similarly, mean shape models of the VS $\bar{x}_{vs}$ and the skull $\bar{x}_{skull}$ are created from $n = 26$ meshes obtained from real patient data. For mean model creation the VS of all 26 CT datasets are automatically segmented, followed by manual validation and improvement to obtain smoother segmentation results. Automated skull segmentation was sufficiently accurate without post-processing.

The SSMs are created by combining the mean models with a gaussian process that represents the possible deformations or shape variations. Any valid shape can be generated by choosing a sufficient parameterization of Eq. (4) as in

$$x_{new} = \bar{x} + \sum_{i=1}^{d} \alpha_i U_i \quad (4)$$

where $U = [U_1, \ldots, U_i] \in \mathbb{R}^{3m \times d}$ contains the shape eigenvectors of the model and $\alpha = [\alpha_1, \ldots, \alpha_i] \in \mathbb{R}^d$ are the coefficients that parameterize the model to form a certain shape [38]. Further, m is the number of vertices of the mean model and d is the number of selected orthonormal basis vectors that form the deformation field of the model [39] and is also referred to as the model's degrees of freedom. Here we chose $d = 50$ for the skull and $d = 200$ for the VS. The higher value of d for the VS is due to the larger variety of shapes, thus requiring a higher number of vectors that form the deformation field. To model the gaussian process, a gaussian kernel is used with $s = 10$ and $\sigma = 40$, where s affects the variance and σ the smoothness of the deformation.

2) Shape Model Fitting: When the mean shape of the SSM is deformed the defined reference points for trepanation and target positions in the VS are simultaneously moved with the deformation of the shape. Shape model fitting is performed using a combined rigid and flexible iterative closest point algorithm. As the SSM are derived from surface meshes the target points are initially defined on the surface of the VS and the skull. To calculate the final placement of the target points inside the left and right VS, two vectors $\vec{KS}_l / \vec{KS}_r$ are constructed from the detected left and right Kocher's points K_l / K_r to the corresponding target points on the surface of the VS S_l^1 / S_r^1. Subsequently, $\vec{KS}_l / \vec{KS}_r$ are extended until the opposite boundary of the VS surface is reached to construct S_l^2 / S_r^2 as illustrated in Fig. 3. Finally, the new target point is

selected at the center of the vector's extension T_l and T_r. The final trajectory is derived as a vector between the left/right Kocher's points and the corresponding target points inside the left/right lateral ventricle calculating $\vec{KT} = \vec{K} - \vec{T}$.

D. Registration of the Marker System to the Patient

Patient movement is visually tracked with the front camera of the HoloLens and a customized marker system that is mounted on the patient's forehead during surgery. In the standard of care (SoC) the patient's head is fully covered with sterile drapes following the transition from the non-sterile to the sterile surgical phase, rendering it impossible to track the patient using visual features. Thus, here we propose tracking the head with a marker system, which consists of four separate parts as shown in Fig. 4a): (1) the head attachment (tripod and mounting plate), (2) the connection to the marker carrier, (3) and the marker carrier with (4) mounted Vuforia markers. The marker system is attached to the patient's forehead. We investigated three different approaches to fix the attachment to the patient's head and to maintain stable positioning: a thermoplastic polymer polycaprolactone that deforms at 42°C and hardens as it cools, a light-curing composite that hardens under UV light, and standard electrocardiogram (ECG) electrode pads on a tripod attachment as depicted in Fig.4a). The third method proved to be most stable and was thus used in further experiments. In addition, an elastic band was used to stabilize the attachment. After assembly of the marker system, precise registration to the patient is crucial. This is performed during the non-sterile phase while the patient head is not covered. Figure 2a) depicts all coordinate systems accounted for in the proposed system. To ensure that the holograms are displayed at the correct position in the AR glasses, the transformation matrix T_H^P between the HoloLens T_H and the patient T_P needs to be continuously derived and updated. During surgery the patient's head is completely covered, while only the marker system is visible. To derive the transformation T_H^P the marker system T_{MS} is tracked continuously and must therefore be registered to the patient. This is achieved in a registration step during which the patient must not be moved. To obtain T_{MS}^P registration from the marker system to the patient is performed by manually placing the patient model precisely over the patient's head in 3D space with the help of a game controller to determine the present position of the patient $T_H^{P_{init}}$. Simultaneously, the marker is tracked to derive the transformation T_H^{MS}. Transformation T_{MS}^P is given by

$$T_{MS}^P = \left(T_H^{MS}\right)^{-1} * T_H^{P_{init}} \tag{5}$$

During the further surgical workflow a stable marker position in relation to the patient's head is assumed, such that tracking the marker results in the position of a patient as in

$$T_H^P = T_H^{MS} * T_{MS}^P. \tag{6}$$

E. Visualization of Holograms

The patient models are superimposed over the patient's head during surgery as depicted in Fig. 4d). Hidden structures are visualized to the surgeon as a navigation aid in the HoloLens, namely the VS, the Kocher's points, and the left and right puncture trajectories. After preprocessing of the data (92s) the generated surface models can be accessed from the AR glasses and used in the further workflow, enabling very fast deployment. Intraoperatively, the surgeon can navigate the catheter in relation to the trajectory to successfully puncture the VS. The representation of the models is developed in close collaboration with three expert neurosurgeons. Different colors and alpha values were tested and evaluated during a user study in the operating room under various light conditions. They can switch on and off visualization of the skull and the

Fig. 4. (a) Experimental setup of a phantom surgery performed on a medical phantom with attached marker system, (b) CAD models of the five used ventricular systems, third and fifth VS are very narrow and third is additionally shifted to the left, (c) expert evaluation, (d) view from HoloLens, (e) puncture results.

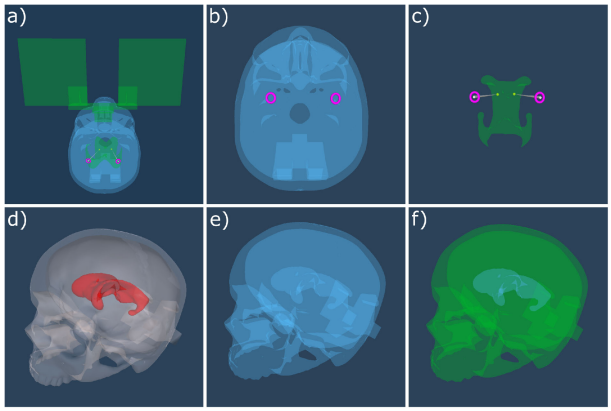

Fig. 5. (a) Final representation of the models in the visualization with included marker system, (b) representation of the Kocher's points in magenta, (c) template with just the VS, the trajectories and optimal points visible, (d-e) different color representations of the patient models that were evaluated in regard to visibility.

optimal trajectories. The minimal visualization is characterized by the display of the VS with the reference points and the marker system to verify the functionality of the tracking (see Fig. 5 a)-c)). The edges of the marker system are highlighted with bright light blue color when the marker is tracked within a frame to visualize a correct tracking to the user. The underlying challenge is to determine a satisfactory balance between visibility, transparency, colors, and their mixing behavior. After the registration of the marker system to the patient a calibration of the HoloLens to the wearer is performed. First the wearers interpupillary distance (IPD) is set in the configuration. The HoloLens 1 does not allow for eye tracking, so the position on the wearer's head must be carefully monitored. The calibration is done by aligning the edges of the virtual marker system with the real physical marker system.

III. Experimental Validation

A. Component Validation

1) Automated Segmentation: The automated segmentation algorithm is evaluated on 26 randomly selected CT datasets from real patients with and without pathologies. To evaluate the accuracy and applicability of the segmentation algorithm as well as its suitability for neurosurgical navigation, results of manually and automatically segmented CT scans are compared. Manual segmentation is performed by two expert neurosurgeons. As shown in Fig. 7c), calcification inside the VS may divide the VS into two independent clusters. As a result, the segmentation of the VS often excludes the posterior sections. However, ventricular puncture in this project is always performed in the frontal section of the VS, which is segmented sufficiently well by the implemented algorithm. Thus, segmentation errors due to calcification in the posterior VS can be neglected for further processing. For the sake of rigour, we evaluate the quality of the segmentation of the section relevant to the proposed application, as well as the complete VS. For quantitative evaluation the Dice Coefficient (F1-Score) is calculated comparing results from manual and automated segmentation.

2) Automated Trajectory Planning: The automated trajectory planning algorithm is evaluated on 33 randomly selected CT datasets from real patients with and without pathologies for both sides, resulting in 66 plannings. In all datasets the Kocher's (K) and target (T) points (refer to Fig. 3) inside the VS are annotated manually by medical experts. A rectangular area of 30×25 mm with the Kocher's point in the center is defined acceptable. Subsequently, the proposed algorithm for point detection automatically identifies the relevant points for both the left and right hemispheres. The derived points are compared to the manual annotation, resulting in an accuracy value that assumes validity of manual annotation. In a next step, results are analyzed whether a point can be categorized as valid, resulting in a reliability metric. Reliability is the value of valid rated points in relation to all determinations. Defining the correct target point in the ventricular system and entry point on the skull is not trivial, thus, every result is rated manually for correctness by experienced medical experts.

3) Marker System and Registration: The overall error of the hologram visualization depends on the re-mounting accuracy of the marker system, the Vuforia marker tracking accuracy and the marker to patient registration accuracy. The mounting error after changing the marker system for the sterile phase was determined using a high precision measuring arm (FARO platinum arm with FARO CAM2 software) with indicated precision of ± 0.037 mm (FARO Technologies Inc., Germany). The evaluation was performed on a commercially available phantom head (Synbone, Switzerland) with an attached silicone skin as shown in Fig. 4a). Measurements were performed on six reference points M_i and P_i $(i = 1, 2, 3)$, three of which located on the marker and the phantom, respectively. A coordinate system is created with the points P_i on the phantom. To obtain positions of M_i, the spherical tip of the FARO measuring arm was placed into indentations at these locations on the marker system. References P_1, P_2 and P_3 are located on the forehead, the cheek and the chin of the phantom, respectively. M_1, M_2 and M_3 are distributed over the removable part of the marker system. The mounting error is determined by comparing positions of the control points M_i in the coordinate space of the phantom. Twenty measurements were taken at each point to determine the mounting repeatability. Three experiments were conducted to evaluate the accuracy of the remounted marker system. In the first experiment E_1 the marker system was changed from the non-sterile to the sterile phase and the measurements were taken. In a second experiment E_2 the phantom was mounted on a Stewart platform (Hexapod, PI GmbH, Germany) and moved randomly in space to mimic small motions that a sedated patient may perform. In the last test E_3, drilling was simulated by holding a wooden plate on the phantom and drilling a hole. Thus, vibrations similar to those occurring during a burr hole trepanation were generated. The measurement uncertainty was obtained by performing 20 measurements on a fixed reference object. According to [40], the accuracy of Vuforia marker tracking is 0.31 ± 0.38 mm. To determine the volumetric registration error, the matching holograms were manually matched to the phantom head using a game controller in 10 experiments. A digital caliper was used to measure the deviation between the holograms and the

phantom separately for each axis. The measurements were performed on three reference points on the custom built phantom to allow an evaluation for all axes over the complete phantom head. Thus, the maximum displacement error inside the phantom where the VS is placed can be determined. Furthermore, this displacement is measured with activated marker tracking using the same metric. If the marker is not visible to the system the holograms remain at the last known position. This again allows the measurement of the displacement error for all axes of the phantom head.

4) Hologram Visualization: The display of holograms was evaluated during a user study under various lighting conditions that may occur in the operating room. In addition, different colors and alpha values were tested for visualization of the holograms. Examples are visualized in Fig. 5d)-f). The colors *red*, *blue*, *green*, *white*, *magenta*, *yellow*, and *orange* were evaluated. Colors were assigned to the models of the VS, targets inside the VS, the skull, the Kocher's points, and the target trajectories.

Processing of the planning algorithms is conducted on a workstation with an Intel i7-9700 CPU, 16GB RAM, SSD and a GeForce 1070 Ti. The utilized AR device is the HoloLens version 1 (Microsoft, USA). Programs for the HoloLens are implemented in Unity 3D (version 2019.1.4f). The HoloLens applications were implemented in C++ and C#, algorithms for automated segmentation and trajectory determination in C++, Python and Scala.

B. Preliminary Experiments

The complete system and clinical procedure were evaluated in a customized head phantom, allowing to integrate various pre-selected VS from real patient data. The shape of the head phantom was created from merged multiple CT scans, see Figure 4c. All boney structures are 3D printed with ASA filament (Stratasys, USA). The phantom head includes a detachable cap in the skull, which may be interchanged and disposed of after each opening of the skull. Additionally, five different interchangable VS may be integrated into the head phantom as presented in Fig. 4e), thus allowing to evaluate the AR navigation system with different healthy and pathological VS (i.e., VS3 and VS5). Here, we chose five VS with various shapes for evaluation, including narrow and asymmetric ones. All VS were previously segmented from real patient data to account for individual and realistic characteristics. The segmented VS are illustrated in Fig. 4b). The customized phantom has a fixed mount for the marker system, such that the transformation T^P_{MS} is known, allowing to separate possible error sources regarding the registration error.

For preliminary evaluation in a laboratory environment, eight non-medical novices with a technical background performed a total of 80 navigated interventions in five different VS with one ventricular puncture into the left and right ventricle, respectively. The investigated task for the subjects included previously fixed registration of the visualized marker and subsequently following the displayed trajectory from Kocher's point towards the target on a VS using a catheter, as illustrated in Fig. 6. During preliminary experimentation, the

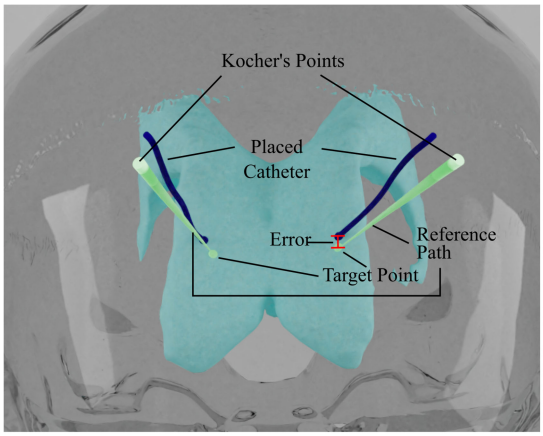

Fig. 6. Visualization of the puncture evaluation with reference path, placed catheter, Kocher's points, target points and penetration error.

subjects were provided with skull caps including a burr hole opening with a diameter of 11 mm, representing the trepanation at the Kocher's point. Like this, focus was laid on the puncture task itself instead of trepanation of the skull.

Each participant punctured five differently shaped VS models in each of the two ventricles, respectively. A mould containing a soft modeling clay is used to represent the VS and disposable skewers are used to puncture. After a successful puncture, the indentation created by the skewer in the model VS is filled with a small amount of modeling clay of a different color. Once participants attempted all punctures, the marked ventricular systems are digitized with a 3D line-scanner (25xx-100, resolution in z: 12 μm, x: 0.15 mm, y: 0.1 mm, Micro-Epsilon, Germany). Comparing the registered digitized ventricular systems and reference images, the indented surface points are extracted. If the VS is penetrated, the surface distance between the optimal puncture point, as defined by the medical experts, and the resulting point, as indented by the participant, is approximated with the standard euclidean distance between the two points. In contrast to the subsequent pre-clinical evaluation, during the preliminary experiments the phantom head did not include a model for brain tissue as here we aimed to investigate general usability of the navigation aid, rather than absolute performance.

A first pre-clinical feasibility study of the AR system was tested on a medical phantom as shown in Fig. 4a. All here presented quantitative and qualitative evaluations were performed on the self-build and designed custom head phantom that is depicted in Fig. 4c and d.

C. Pre-Clinical Evaluation

After proving general feasibility for neurosurgical navigation in the preliminary experiments, the performance of the complete system and its ability to aid during neurosurgical instrument navigation is experimentally evaluated in a clinical scenario. For this, neurosurgical experts conducted complete ventriculostomies with and without augmented reality support. For the experiments, the custom phantom heads (compare Section III-B) were filled with agar gel at a concentration of 0.5% that when cooled and hardened resembles brain tissue [41]. In contrast to the preliminary navigation

experiments, the addition of model brain tissue restricts corrective motion of the catheter once inside the head, and thus, emulates a real surgery. The VS is represented with modeling clay in the shape of five individual ventricular systems as shown in Fig. 4b) and e).

Prior to catheter insertion, the surgeons had to locate the left and right Kocher's points on the model skull (see Fig. 3) and drill a trepanation hole at each of these points to gain access to the brain. The trepanation holes are drilled into replaceable skull plates with a surgical drill (Stryker Corp., Kalamazoo, Michigan, USA) with a diameter of 11 mm. After opening the skull, a standard of care reinforced catheter is navigated through the burr hole and agar towards a target on the respective ventricle. The same five ventricle shapes are used as in the preliminary experiments.

During the pre-clinical evaluation of the navigation aid, a total of seven neurosurgeons and three neurosurgical residents performed ten ventriculostomies each, utilizing the augmented reality system, as illustrated in Fig. 4c). Throughout the procedure, the surgeons wore the AR-glasses to visualize the Kocher's points for correct trepanation, the target on the respective ventricle and the optimized trajectory for catheter placement. The object visualizations could be changed at will using an XBox controller (Microsoft Corp., Redmont, WA, USA) to chose between different presented anatomical structures, i.e., VS, skin, skull, reference path. Subsequently, the surgeon could insert the catheter manually under visual guidance along the presented path towards the target. In the first trial, each of 10 participating surgeons performed a total of 10 ventricular punctures in five different ventricular systems, i.e., $n_1 = 100$. During a subsequent second trial, 2 neurosurgeons and two neurosurgical residents performed another 8 procedures in the same five VS, i.e., a total of $n_2 = 80$ ventricular punctures. The second trial was performed to investigate the influence of experience with AR on the qualitative outcome of the procedure. For control experiments, 6 surgeons (5 neurosurgeons and 1 neurosurgical resident) conducted a total of $n_c = 60$ ventriculostomies similar to the standard of care without the aid of augmented reality. Therefore, planning of the catheter placement was performed using the in-house medical imaging system. In both studies, after a surgeon performed punctures in the left and right ventricles of all five ventricular systems, respectively, the phantom heads are digitized utilizing a medical CT scanner (Siemens Healthcare, Erlangen, Germany). From the digitized VS, the surface distance between the optimal puncture point and the achieved point where the catheter penetrates the VS surface is approximated by the standard euclidean distance between these points, as illustrated in Fig. 6.

After the pre-clinical experiments aided by AR navigation, the participating surgeons filled out a questionnaire to determine their level of acceptance and usability of the AR-based assistance for ventriculostomy.

IV. Results

A. Automated Segmentation

Results of the automated segmentation are compared to a manually segmented ground truth. Two examples of segmented VS are illustrated in Fig. 7a) and b). Calcification in the VS may lead to detection of several clusters, and thus, inaccurate segmentation of the complete VS, as seen in Fig. 7c). To account for this limitation, segmentation of the partial VS are performed. As calcification usually are found in the posterior part of the ventricles, which are not targeted during venriculostomy, these may be neglected for further processing. The Dice (F1) scores for segmentation of complete and partial (i.e., neglecting calcification) ventricular systems are presented in Table I. The overall runtime of the automated segmentation is 2.3±0.2 s per structure leading to 6.9±0.6 s segmentation time for all structures.

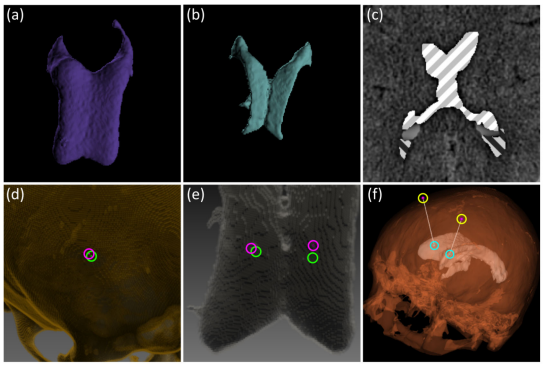

Fig. 7. (a-b) Results of segmented ventricular systems, (c) a VS divided by calcifications into frontal (top) and posterior (bottom) sections, (d) determination of a Kocher's point, (e) target point inside the VS - green: annotated point, violet: determined point and (f) complete puncture trajectory.

TABLE I
Comparison Between Automatic and Manual Segmentation of (a) the Complete and (b) the Partial VS

	VS1		VS2		VS3		VS4	
	(a)	(b)	(a)	(b)	(a)	(b)	(a)	(b)
F1-Score	0.93	0.95	0.91	0.99	0.85	0.99	0.84	0.99

B. Automated Trajectory Planning

Results for automated trajectory planning are depicted in Fig. 7d) to f). The Kocher's points are determined correctly inside the optimal area with a mean accuracy of 8.4±4.5 mm ($n = 66$) and a reliability of 98.4%. The resulting errors in x-, y-, and z-directions as well as the absolute error are depicted in detail in Fig. 8a) to d). For determination of the target points inside the VS in relation to the optimal trepanation point (see Fig. 7e) a mean error 4.9±2.3 mm is reached with a reliability of 95.4%. The resulting errors in x-, y-, and z-directions as well as the absolute error are illustrated in Fig. 8 e) to h). A valid trajectory is planned in 93.9% of cases. The overall runtime of the automated trajectory determination is 57.0±3.4s (nrrd to stl conversion: 19s, Kocher's point determination: 18s, target point determination inside the VS: 15s, trajectory calculation and model generation: 5s). If the algorithm fails to detect all points accurately, the procedure allows for human intervention and adjustment by the responsible surgeon.

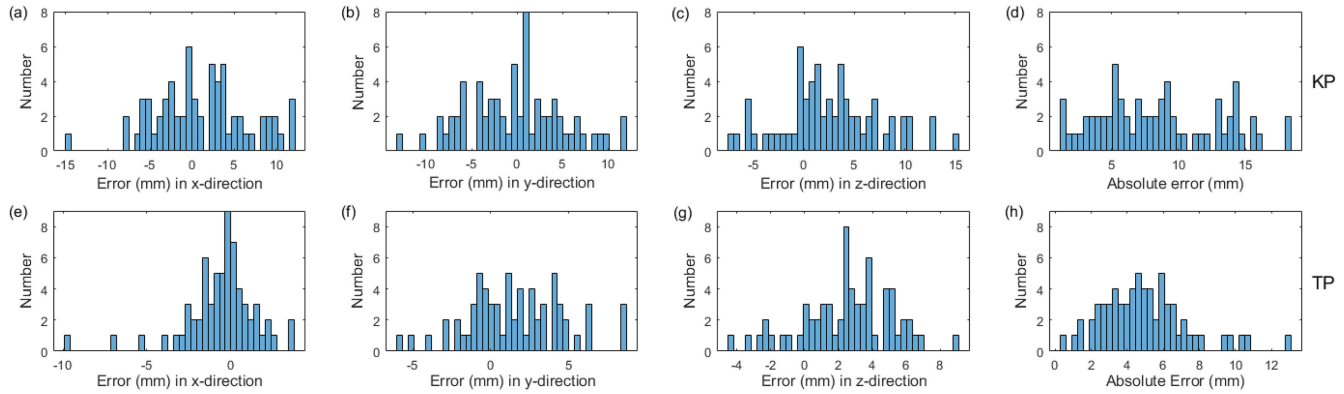

Fig. 8. (a) Error [mm] of automated determination of the Kocher's point on the skull: in x-direction, (b) y-direction, (c) z-direction and (d) absolute error. (e) Error [mm] of automated determination of the target point inside the VS: in x-direction, (f) y-direction, (g) z-direction and (h) absolute error.

TABLE II
MOUNTING ERROR ON REFERENCE POINTS M_1, M_2, M_3. E_1: STATIC PHANTOM, NO MOVEMENT. E_2: SLIGHT RANDOM MOTION. E_3: DRILLING SIMULATION. (ALL VALUES IN MM)

	E_1	E_2	E_3	Mean(M_i)	SD(M_i)
M_1	0.17	0.16	0.16	0.16	0.06
M_2	0.21	0.18	0.16	0.19	0.06
M_3	0.23	0.16	0.17	0.19	0.06
Mean(E_i)	0.20	0.17	0.17	0.18	-
SD(E_i)	0.08	0.05	0.04	-	0.06

C. Marker System and Registration

Accuracy of the remounted marker system yielded uncertainties with a mean value of 0.18±0.06 mm considering all experiments E_1, E_2 and E_3 as summarized in Table II.

The Vuforia marker was tracked at an average speed of 23-26 frames per second, which results in a stable display of the holograms. Nevertheless, a delay is noticeable, especially when the patient or the surgeon move quickly. The following mean error values were identified for volumetric registration of the hologram to the head phantom: 1.36±1.33 mm for the x-axis, 1.45±0.87 mm for the y-axis, and 1.19±0.83 mm for the z-axis. The volumetric mean error over all axes was 2.71±1.18 mm. The time to perform the complete registration was evaluated as 100.5±63.5 s, depending strongly on the user's experience with the system. The hologram registration experiments with enabled marker system tracking yielded an accuracy of 2.91±1.47 mm. This includes the registration error (2.71±1.18 mm) and the tracking error for Vuforia markers confirming measurements by Kiss *et al.* [40]. The sum of all three influencing error values (remount, registration and Vuforia marker tracking error [40]) results in a total volumetric error of the marker system of 3.2±1.62 mm.

D. Hologram Visualization

The holograms were visualized under normal OR light conditions as illustrated in Fig. 4d). Visualization problems become apparent when the surgical lighting shines directly on the visor of the HoloLens as the holograms are no longer visible. Preferred visualization was achieved with slightly dimmed lighting, guaranteeing the simultaneous visibility of the holograms and the operating room.

User studies yielded in the combination of assigned colors with best visibility: skull - *blue*, ventricular system - *green*, Kocher's points - *magenta*, trajectories - *white*, and targets - *yellow*. An alpha value of 0.5 was selected. In addition, the user may adjust brightness by controlling the hardware buttons.

The HoloLens was designed to operate in a range of 1 to 2 meters, which guarantees an optimal visualization of the holograms. Our system operates in ranges of 50-80cm. No additional problems were encountered in that range, besides the small field of view. One problem that can occur is, that the holograms are perceived as floating above the phantom. Therefore, it is preferable to use low brightness so that the holograms and the real world can be seen simultaneously to minimize this issue.

E. Preliminary Experiments

The mean accuracy, standard deviation and overall success rates for punctures of left and right ventricles of the five VS are summarized in Table III. The mean error of all ventricular punctures during preliminary experimentation is found to be 5.6 ± 2.8 mm with an average success rate of 91.25%. The highest mean error (8.8±3.1 mm) occurred during puncture of the left ventricle of the third VS. This VS represents a pathological structure with an asymmetric narrow shape. The lowest mean error occurrence (4.0 ± 1.8 mm) was found for punctures into the right ventricle of the second VS, representing a relatively large VS. The lowest success rate (62.5%) occurred when puncturing the right ventricle of the fifth VS with very narrow ventricles. Qualitative evaluation of the navigation aid during preliminary experiments included good acceptance by the subjects due to (1) the clear visualization of the anatomical structures with no visual clutter, (2) the adjustable brightness, and (3) the intuitive control of the system. On the other hand, users complained about a relatively small field of view and a unsatisfactory contrast of colors in the visualization.

F. Pre-Clinical Evaluation

The mean error, standard deviation, and overall success rate for ventriculostomies, as well as determination of the Kocher's point, with and without augmented reality navigation aid are

TABLE III
ACCURACY, SD AND OVERALL SUCCESS RATE OF PRELIMINARY EXPERIMENTS WITH NOVICE USERS FOR ALL 5 VS (LEFT AND RIGHT VENTRICLES)

Novice	VS1L	VS1R	VS2L	VS2R	VS3L	VS3R	VS4L	VS4R	VS5L	VS5R	ALL VS
Mean Error (mm)	6.0	5.6	5.4	4.0	8.8	5.4	5.5	4.3	5.4	4.9	5.6
Standard Deviation (mm)	3.6	2.9	2.3	1.8	3.1	2.8	1.4	1.9	1.6	4.7	2.8
Success-Rate (%)	87.50	100	100	87.5	100	87.5	100	100	87.50	62.50	91.25

TABLE IV
ACCURACY, SD AND OVERALL SUCCESS RATE OF THE CONTROL GROUP WHO PERFORMS THE INTERVENTION WITH THE STANDARD OF CARE (SOC) WITHOUT AR AND AR-GUIDED EVALUATION FOR ALL 5 VS (LEFT AND RIGHT VENTRICLES) AND KOCHER'S POINT (K)

SoC ($n_c = 60$)	VS1L	VS1R	VS2L	VS2R	VS3L	VS3R	VS4L	VS4R	VS5L	VS5R	ALL VS	K
Mean Error (mm)	9.5	6.7	5.0	6.2	6.3	5.6	6.1	5.8	7.2	6.1	6.5	8.2
Standard Deviation (mm)	2.3	3.0	1.9	2.9	2.4	1.3	2.6	2.1	2.0	1.6	2.4	2.8
Success-Rate (%)	83.3	83.3	100	66.7	83.33	50.00	100.00	66.67	50	33.33	71.7	100
AR-guided ($n_{AR} = 180$)	VS1L	VS1R	VS2L	VS2R	VS3L	VS3R	VS4L	VS4R	VS5L	VS5R	ALL VS	K
Mean Error (mm)	3.9	4.6	5.0	5.8	5.4	4.4	5.7	4.7	4.1	3.6	4.8	5.4
Standard Deviation (mm)	1.5	2.3	3.0	2.7	3.4	2.7	2.1	2.3	1.8	2.0	2.5	2.4
Success-Rate (%)	88.9	88.9	100	83.3	72.2	55.6	94.44	88.9	88.9	55.6	81.7	100

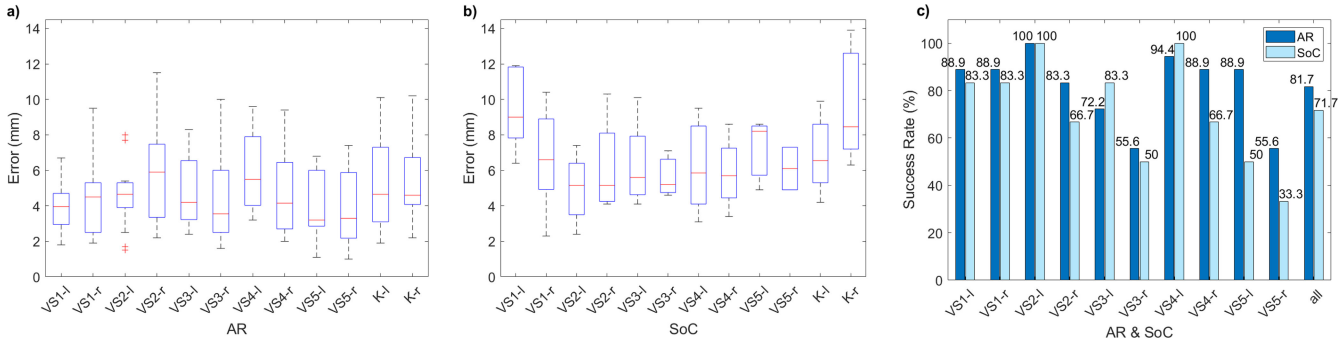

Fig. 9. (a) Resulting boxplots for experimental validation by experts AR-guided and (b) following the standard of care (SoC) and (c) puncture success rates.

presented in Table IV and illustrated in Fig. 9. The success rate determines whether the targeted ventricle has been punctured. The mean error for AR-supported ventriculostomy is 4.8 ± 2.5 mm with an average success rate of 81.7%. Control experiments, i.e., ventricular puncture similar to the standard of care and without AR navigation, show a higher mean error of 6.5 ± 2.4 mm with an overall success rate of 71.67%. Here, the presented data for AR-guided interventions include results from both trials 1 and 2. If neglecting results from trial 2, i.e., with initial training, the mean error increases to 5.3 ± 2.6 mm with a decreased average success rate of 73.0% compared to an average of all conducted AR-supported punctures. However, solely focusing on results from trial 2 ($n_2 = 80$), the mean error drops to 4.3 ± 2.2 mm with an overall success rate of 92.5% as only two ventricles were not successfully penetrated during trial 2. Further, Table IV shows that the Kocher's point (K) was successfully determined in 100% of all cases. However, the resulting mean error for the control group (8.2 ± 2.8 mm) is significantly higher than that of interventions performed with AR navigation (4.8 ± 2.5 mm).

Additionally, during the study with neurosurgical experts quantitative evaluation data of the navigation aid were gathered and allowed to analyse acceptability and user satisfaction. Results are summarized in Fig. 10. The chart shows that 85.7% of participating surgeons approve the convenience of the navigation aid (*strongly agree* or *agree*) and 92.9% think that the system has the potential to improve accuracy of cranial procedures. However, a lower proportion of surgeons (64.2%)

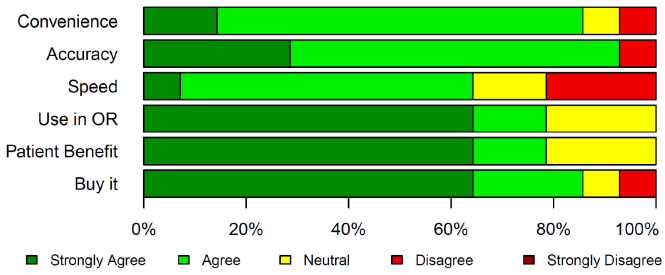

Fig. 10. Results of expert user acceptance survey for the AR navigation aid (ARNA). Users answered to statements on a 5 point Likert scale: 1) ARNA is convenient, 2) ARNA improves accuracy of ventriculostomy, 3) ARNA speeds up my workflow, 4) I would use ARNA in the OR, 5) My patients would benefit from ARNA, and 6) If ARNA was a product I would buy it.

believe that usage of AR-support would speed up the surgical workflow. Further, 78.6% of the interviewed surgeons would use the navigation aid in the OR and believe that patients would benefit from the system. Summarizing, 85.7% would consider buying this technology if it was a marketed product.

V. DISCUSSION

The quality and robustness of the segmentation of cranial structures depends on several factors such as the resolution of the imaging modality and the existence of various types of pathologies, such as hematoma or calcification of the plexus choroideus. The proposed algorithm achieves very good segmentation results with a dice coefficient (F1 score) of more than 98%. Additionally, the presented approach is able to

detect blood clots inside the VS and adjusted versions can be used to segment the skull and the skin.

The automated trajectory planning was implemented using statistical shape models, which form a powerful tool to model shape classes and their deformations. In 93.9%, the proposed algorithm determined a valid path. Anytime in the process, a surgeon may intervene and adjust the burr hole and target point positions to react to special circumstances. Preprocessing of data is essential due to ambiguities contained in the CT data, such as misalignment and orientation of the patient, pathologies, and noise in the data. Future work will combine the proposed approach with a dedicated landmark detection to orient the patient correctly. An alternative approach is using a variety of shape models with adapted orientations. The shape models could also be expanded by landmarks as correspondence points. Further considerations include a better processing capability for various pathologies, especially when the head is strongly damaged or deformed caused by traumatic brain injury.

The hologram visualization error was determined as 3.2 ± 1.62 mm, which is surgically sufficient for ventriculostomies. The initial evaluation included a fixed marker to patient registration as it would be the case if fiducial markers are attached to the patient prior the CT, which is in many systems the standard of care. A possible additional deviation is mainly caused through a manual registration error in x-direction of 1.36 ± 1.33 mm. See the illustrated coordinate system in Fig. 3a).

A surgeon normally looks directly into the puncture path making the error in z-direction negligible. Due to the elongated shape of the VS that follows the y-direction, errors on this axis are also less significant. Even when including the additional error in x-direction, the deviation seems acceptable in most cases for the pre-clinical experiments. We will examine this in future work, now that possible error sources have been separated. Preliminary experiments demonstrated the feasibility of AR-guided ventriculostomies and showed a high success rate of 91.25%. However, puncturing through air seems much simpler than through an agar filled phantom head. In a pre-clinical evaluation, two experiments were carried out. In the first one 180 ventricular punctures were carried out with AR-guidance. Additionally, a control study was conducted comparable to the standard of care with 60 ventriculostomies on five phantom heads and 10 ventricles, respectively. The AR-guided ventriculostomies yielded a ten percent higher success rate of 81.7% and an overall better puncture accuracy of 4.8 ± 2.5 mm, while the control group achieved an average accuracy of 6.5 ± 2.4 mm. Thus, a significant improvement for AR-guided catheter placement during ventriculostomy could be demonstrated.

The haptic feedback differs significantly to a real procedure, in which a loss of resistance is present when entering the ventricle as well as an immediate drainage of CSF in most cases. The modelling clay, however, leads to a subtle increase of resistance. Furthermore, the test setup did not allow surgeons to correct the trajectory they initially chose. These factors combined with using new, unfamiliar hardware may have interfered with the performance. For most participating surgeons these experiments were the first experience with surgical navigation using AR through a head mounted display. Further experiments with trained expert participants show improved results, suggesting a steep learning curve. Two of the selected VS posed a major challenge due to their relatively small volume (see Fig. 4 b). Two of which were derived from CT-scans with a 1.5 cm midline-shift to the left side (the third VS) and one with two very narrow ventricles (the fifth VS). This may account for the worst results in terms of success rate of only 55.6%.

In neurosurgical practice ventriculostomies are not often indicated in patients with an intracranial pathology that leads to a significant midline shift. The aim of this study was to include puncture targets that are particularly challenging, such as a displaced ventricle. As a result, the ventricular drain's angle of entrance differs significantly from a routine case, thus differing from routine practice. The results reflect clinical experience, in which a displaced, compressed or narrow VS is more challenging to hit. A possibility for the system to overcome this limitation is to automatically detect shifts and narrow ventricles and indicate these to surgeons by providing visual aid, so that surgeons may adjust their approach. In our experiments, VS3-r and VS5-r seem particularly challenging to puncture due to the midline-shift and narrow ventricles. When ignoring results from VS3, the neurosurgical experts achieve a higher mean success rate of 88.2% for the remaining VS, instead of 81.7% (all VS). Further, when puncturing through agar gel, the trajectory is restricted after entering the phantom head and movement is reduced to one degree of freedom, i.e., forward motion.

The additional determination of the Kocher's points was not observed to influence the puncture error on the surface of the VS to a large extent. Even if the trepanation point into the skull differs, the target point inside the VS is still displayed correctly from only a slightly different point of view. This emphasizes the robustness of the system. The observation also correlates to the fact that the Kocher's point is not precisely defined in neurosurgery, but rather a Kocher's area is specified, as shown in Fig. 3b). A post-experimental participant survey overall reveals positive feedback. One major challenge that affected some of the participants, however, were difficulties when focusing on the surgical procedure and the hologram alternately. Some users complained about slight headaches towards the end of the experiment. This observation is presumably due to perceptual limitations of the AR lens as the holograms are displayed on a visor in front of the eyes resulting in unnatural and unintuitive image perception as shown in [42]. Presumably the biggest source of error is the training status of a user, their experience with augmented reality, and the correct interaction with the visualization aid that is provided. Further investigations will focus on more intuitive user guidance.

VI. Conclusion

This work presents an automated system for AR guided neurosurgical interventions on the example of the ventricular puncture. The system considers automation of the

complete surgical process from planning to operative surgical navigation. Individualized anatomical patient models are generated automatically from CT data to segment the skin, the skull, and the ventricular system. Based on the patient-specific anatomy a surgical trajectory is planned. At any time in the surgical workflow the surgeon can interact with the system to make adjustments in order to obtain ideal surgical support. A marker system meeting the procedural requirements is developed for intraoperative patient tracking that additionally supports the change from the non-sterile to the sterile surgical phase. Expert evaluation of the system in a realistic surgical setting results in a success rate of 81.7% with mean accuracy of 4.8±2.5 mm.

REFERENCES

[1] T. J. Wilson, W. R. Stetler, Jr., W. N. Al-Holou, and S. E Sullivan, "Comparison of the accuracy of ventricular catheter placement using freehand placement, ultrasonic guidance, and stereotactic neuronavigation," *J. Neurosurg.*, vol. 119, no. 1, pp. 66–70, 2013.

[2] A. K. Toma, S. Camp, L. D. Watkins, J. Grieve, and N. D. Kitchen, "External ventricular drain insertion accuracy: Is there a need for change in practice?" *Neurosurgery*, vol. 65, no. 6, pp. 1197–1201, 2009.

[3] C. R. P. Lind, A. M. C. Tsai, C. J. Lind, and A. J. J. Law, "Ventricular catheter placement accuracy in non-stereotactic shunt surgery for hydrocephalus," *J. Clin. Neurosci.*, vol. 16, no. 7, pp. 918–920, 2009.

[4] U. K. Kakarla, L. J. Kim, S. W. Chang, N. Theodore, and R. F. Spetzler, "Safety and accuracy of bedside external ventricular drain placement," *Oper. Neurosurg.*, vol. 63, no. 1, pp. ONS162–ONS167, 2008.

[5] D. R. Huyette, B. J. Turnbow, C. Kaufman, D. F. Vaslow, B. B. Whiting, and M. Y. Oh, "Accuracy of the freehand pass technique for ventriculostomy catheter placement: Retrospective assessment using computed tomography scans," *J. Neurosurg.*, vol. 108, no. 1, pp. 88–91, 2008.

[6] C.-C. Hsia *et al.*, "The misplacement of external ventricular drain by freehand method in emergent neurosurgery," *Acta Neurologica Belgica*, vol. 111, no. 1, pp. 22–28, 2011.

[7] C. Raabe, J. Fichtner, J. Beck, J. Gralla, and A. Raabe, "Revisiting the rules for freehand ventriculostomy: A virtual reality analysis," *J. Neurosurg.*, vol. 128, no. 4, pp. 1250–1257, 2018.

[8] P. M. Foreman, P. Hendrix, C. Griessenauer, P. G. R. Schmalz, and M. Harrigan, "External ventricular drain placement in the intensive care unit versus operating room: Evaluation of complications and accuracy," *Clin. Neurol. Neurosurg.*, vol. 128, pp. 94–100, Jan. 2015.

[9] B. R. O'Neill, D. A. Velez, E. E. Braxton, D. Whiting, and M. Y. Oh, "A survey of ventriculostomy and intracranial pressure monitor placement practices," *Surg. Neurol.*, vol. 70, no. 3, pp. 268–273, 2008.

[10] T. Rehman *et al.*, "A radiographic analysis of ventricular trajectories," *World Neurosurg.*, vol. 80, nos. 1–2, pp. 173–178, 2013.

[11] J. S. Beckett *et al.*, "Autonomous trajectory planning for external ventricular drain placement," *Oper. Neurosurg.*, vol. 15, no. 4, pp. 433–439, 2018.

[12] X. Qian *et al.*, "Objective ventricle segmentation in brain CT with ischemic stroke based on anatomical knowledge," *BioMed Res. Int.*, vol. 2017, Feb. 2017, Art. no. 8690892.

[13] H. Schnack, H. E. H. Pol, W. F. Baaré, M. A. Viergever, and R. S. Kahn, "Automatic segmentation of the ventricular system from MR images of the human brain," *Neuroimage*, vol. 14, no. 1, pp. 95–104, 2001.

[14] W. Chen, R. Smith, S.-Y. Ji, K. R. Ward, and K. Najarian, "Automated ventricular systems segmentation in brain CT images by combining low-level segmentation and high-level template matching," *BMC Med. Inform. Decis. Making*, vol. 9, no. S1, p. S4, 2009.

[15] A. S. Lundervold and A. Lundervold, "An overview of deep learning in medical imaging focusing on MRI," *Zeitschrift Medizinische Physik*, vol. 29, no. 2, pp. 102–127, 2019.

[16] A. Meola, F. Cutolo, M. Carbone, F. Cagnazzo, V. Ferrari, and M. Ferrari, "Augmented reality in neurosurgery: A systematic review," *Neurosurg. Rev.*, vol. 40, no. 4, pp. 537–548, 2017.

[17] B. Czupryński and A. Strupczewski, "High accuracy head pose tracking survey," in *Proc. Int. Conf. Active Media Technol.*, 2014, pp. 407–420.

[18] E. Murphy-Chutorian and M. M. Trivedi, "Head pose estimation in computer vision: A survey," *IEEE Trans. Pattern Anal. Mach. Intell.*, vol. 31, no. 4, pp. 607–626, Apr. 2009.

[19] Y. Wu and Q. Ji, "Facial landmark detection: A literature survey," *Int. J. Comput. Vis.*, vol. 127, no. 2, pp. 115–142, 2019.

[20] E. Olson, "AprilTag: A robust and flexible visual fiducial system," in *Proc. IEEE Int. Conf. Robot. Autom.*, 2011, pp. 3400–3407.

[21] S. Garrido-Jurado, R. Muñoz-Salinas, F. J. Madrid-Cuevas, and M. J. Marín-Jiménez "Automatic generation and detection of highly reliable fiducial markers under occlusion," *Pattern Recognit.*, vol. 47, no. 6, pp. 2280–2292, 2014.

[22] C. Kunz, V. Genten, P. Meißner, and B. Hein, "Metric-based evaluation of fiducial markers for medical procedures," in *Medical Imaging 2019: Image-Guided Procedures, Robotic Interventions, and Modeling*, vol. 10951. Bellingham, WA, USA: SPIE, 2019, pp. 690–703.

[23] T. Frantz, B. Jansen, J. Duerinck, and J. Vandemeulebroucke, "Augmenting Microsoft's HoloLens with vuforia tracking for neuronavigation," *Healthcare Technol. Lett.*, vol. 5, no. 5, pp. 221–225, 2018.

[24] R. A. Kockro *et al.*, "Dex-ray: Augmented reality neurosurgical navigation with a handheld video probe," *Neurosurgery*, vol. 65, no. 4, pp. 795–808, 2009.

[25] L. B. Tabrizi and M. Mahvash, "Augmented reality–guided neurosurgery: Accuracy and intraoperative application of an image projection technique," *J. Neurosurg.*, vol. 123, no. 1, pp. 206–211, 2015.

[26] P. Hübner, K. Clintworth, Q. Liu, M. Weinmann, and S. Wursthorn, "Evaluation of HoloLens tracking and depth sensing for indoor mapping applications," *Sensors*, vol. 20, no. 4, p. 1021, 2020.

[27] R. Vassallo, A. Rankin, E. C. S. Chen, and T. M. Peters, "Hologram stability evaluation for microsoft hololens," in *Medical Imaging 2017: Image Perception, Observer Performance, and Technology Assessment*, vol. 10136. Bellingham, WA, USA: Int. Soc. Opt. Photon., 2017, Art. no. 1013614.

[28] J. W. Meulstee *et al.*, "Toward holographic-guided surgery," *Surg. Innov.*, vol. 26, no. 1, pp. 86–94, 2019.

[29] J. T. Gibby, S. A. Swenson, S. Cvetko, R. Rao, and R. Javan, "Head-mounted display augmented reality to guide pedicle screw placement utilizing computed tomography," *Int. J. Comput. Assist. Radiol. Surgery*, vol. 14, no. 3, pp. 525–535, 2019.

[30] Y. Li *et al.*, "A wearable mixed-reality holographic computer for guiding external ventricular drain insertion at the bedside," *J. Neurosurg.*, vol. 131, no. 5, pp. 1599–1606, 2018.

[31] E. Azimi *et al.*, "An interactive mixed reality platform for bedside surgical procedures," in *Medical Image Computing and Computer Assisted Intervention (MICCAI)*, A. L. Martel *et al.*, Eds. Cham, Switzerland: Springer, 2020, pp. 65–75.

[32] E. Rae, A. Lasso, M. Holden, E. Morin, R. Levy, and G. Fichtinger, "Neurosurgical burr hole placement using the microsoft HoloLens," in *Medical Imaging 2018: Image-Guided Procedures, Robotic Interventions, and Modeling*, vol. 10576. Bellingham, WA, USA: Int. Soc. Opt. Photon., 2018, Art. no. 105760T.

[33] M. S. Labini, C. Gsaxner, A. Pepe, J. Wallner, J. Egger, and V. Bevilacqua, "Depth-awareness in a system for mixed-reality aided surgical procedures," in *Proc. Int. Conf. Intell. Comput.*. 2019, pp. 716–726.

[34] F. Cutolo *et al.*, "A new head-mounted display-based augmented reality system in neurosurgical oncology: A study on phantom," *Comput. Assist. Surgery*, vol. 22, no. 1, pp. 39–53, 2017.

[35] SourceForge-Teem. (Mar. 9, 2021). *Definition of NRRD File Format*. [Online]. Available: http://teem.sourceforge.net/nrrd/format.html

[36] C. Kunz *et al.*, "Fast volumetric auto-segmentation of head ct images in emergency situations for ventricular punctures," in *Proc. CURAC*, 2019, pp. 41–46.

[37] G. Bouabene *et al.*, (2016). *Scalismo Framework*. Accessed: Mar. 9, 2021. [Online]. Available: https://scalismo.org/

[38] J. Booth, A. Roussos, S. Zafeiriou, A. Ponniah, and D. Dunaway, "A 3D morphable model learnt from 10,000 faces," in *Proc. IEEE Conf. Comput. Vis. Pattern Recognit.*, 2016, pp. 5543–5552.

[39] M. Lüthi, T. Gerig, C. Jud, and T. Vetter, "Gaussian process morphable models," *IEEE Trans. Pattern Anal. Mach. Intell.*, vol. 40, no. 8, pp. 1860–1873, Aug. 2018.

[40] G. Kiss, C. L. Palmer, and H. Torp, "Patient adapted augmented reality system for real-time echocardiographic applications," in *Proc. Workshop Augmented Environ. Comput. Assist. Intervent.*, 2015, pp. 145–154.

[41] Z.-J. Chen *et al.*, "A realistic brain tissue phantom for intraparenchymal infusion studies," *J. Neurosurg.*, vol. 101, no. 2, pp. 314–322, 2004.

[42] S. Condino, M. Carbone, R. Piazza, M. Ferrari, and V. Ferrari, "Perceptual limits of optical see-through visors for augmented reality guidance of manual tasks," *IEEE Trans. Biomed. Eng.*, vol. 67, no. 2, pp. 411–419, Feb. 2020.